Materials Advances

ROYAL SOCIETY OF CHEMISTRY

PAPER

View Article Online
View Journal | View Issue

Cite this: *Mater. Adv.*, 2022, 3, 437

Nanoparticles sandwiched in hollow amorphous metal–organic frameworks with enhanced diffusion for highly selective benzene oxidation†‡

Vijayan Srinivasapriyan [ab]

Received 27th August 2021,
Accepted 7th October 2021

DOI: 10.1039/d1ma00768h

rsc.li/materials-advances

Efficient and selective catalysts are pivotal for the chemical industry. The functionalization of benzene plays a vital role in the petrochemical industry by converting benzene into other value-added chemicals, such as phenols, anilines, *etc.* In the chemical industry, phenol production is based on the three step cumene process, which produces hazardous cumene hydroperoxide as an intermediate and also equimolar acetone as a coproduct. So, the direct oxidation of benzene to phenol is desirable. Unfortunately, most of the developed catalysts require an elevated temperature and suffer from low conversion. So, here we designed a series of hollow amorphous nanomaterials, based on aMIL-100 with metal nodes of Fe, Cr, Al and Sc, by sandwiching nanoparticles, such as Pt, Rh and Ru, in between hollow amorphous metal–organic frameworks with enhanced diffusion for highly selective benzene oxidation. We have achieved 52% benzene conversion and 99.5% selectivity for phenol.

Introduction

Over the last 25 years, reticular chemistry has enabled tremendous advances in the field of porous materials.[1–4] In particular, metal–organic frameworks (MOFs) are one of the most fascinating materials in reticular chemistry and demonstrate a myriad of applications in areas such as catalysis,[5–10] water harvesting,[11–13] adsorption,[14] separation,[15] energy[16,17] and electronics.[18,19] Moreover, hollow[20–25] and amorphous or hierarchical MOFs[26–29] have attracted intensive attention due to their unique architecture, with good permeation, large enclosed cavities, thin shells and low density, as well as their inherent properties from the MOFs. These may serve as a new platform for the exploration of novel applications. For example, Liu *et al.* reported that multi-shelled hollow MIL-101 crystals show enhanced catalytic oxidation of styrene relative to that of the solid nanocrystals.[30] Qin *et al.* reported that a hollow mesoporous MOF with a hollow macroporous core and mesoporous shell exhibits highly efficient catalytic properties toward benzyl alcohol oxidation.[31]

Phenol, one of the most important chemicals in the petrochemical industry,[32] has been synthesised based on the cumene process, which produces hazardous cumene hydroperoxide as an intermediate as well as equimolar acetone as a coproduct.[33] So, the direct and selective oxidation of benzene is an attractive and challenging method for phenol production.[34,35] This direct oxidation can be achieved by various oxidants, such as O_2,[36,37] N_2O,[38–40] and H_2O_2.[41–45] In particular, the H_2O_2 oxidant process is environmentally green due to only producing water as a by-product. However, the direct C–H activation of benzene is a more challenging one. Until now, all the developed catalysts require an elevated temperature and suffer from low conversion because of the notoriously low reactivity of C–H bonds and, especially under heating conditions, phenol is easily overoxidized to yield products such as *p*-benzoquinone. So, we designed a series of hollow sandwich nanostructures based on aMIL-100 (amorphous MIL-100) with metal nodes of Fe, Cr, Al and Sc connected with 1,3,5-benzene tricarboxylate (BTC) which were rationally synthesized using monodisperse polystyrene (PS) nanoparticles as templates through a versatile step-by-step self-assembly strategy.[46] Sandwiching nanoparticles between an inner hollow aMOF and an outer shell composed of an aMOF leads to highly stable and selective catalysts for the oxidation of benzene to phenol at room temperature. Due to the low density of hollow aMOFs, the amount of catalyst loading is reduced to 2 mg instead of the 20 to 50 mg of solid

[a] *CAS Key Laboratory of Nanosystem and Hierarchical Fabrication, CAS Center for Excellence in Nanoscience, National Center for Nanoscience and Technology, Beijing, 100190, China. E-mail: vsripriyan@mails.ucas.edu.cn*
[b] *School of Nanoscience and Technology, University of Chinese Academy of Sciences, Beijing, 100049, China*

† Dedicated to Professor Zhiyong Tang on the occasion of his 50th birthday.

‡ Electronic supplementary information (ESI) available. See DOI: 10.1039/D1MA00768H

Table 1 Catalytic reactions of benzene to phenol using various catalysts

Entry	Catalysts	Time	Conversion	Selectivity
1	Pt or Rh or Ru NPs	12	—	—
2	HMIL-100(Fe)	12	13	56
3	MIL-100(Fe) solid	12	7.3	75
4	HMIL-100(Al)@Pt	12	3.0	48
5	HMIL-100(Sc)@Pt	12	2.0	33
6	HMIL-100(Cr)@Pt	12	6.0	46
7	HMIL-100(Fe)@Pt	12	35	99
8	HMIL-100(Al)@Pt@aMIL-100(Al)	12	4.9	45
9	HMIL-100(Sc)@Pt@aMIL-100(Sc)	12	4.0	26
10	HMIL-100(Cr)@Pt@aMIL-100(Cr)	12	9.0	42
11	HMIL-100(Fe)@Pt@aMIL-100(Fe)	12	52	99.5
12	HMIL-100(Fe)@Rh@aMIL-100(Fe)	12	78	68
13	HMIL-100(Fe)@Ru@aMIL-100(Fe)	12	38	73

Reaction conditions: benzene (0.40 mL), 6 mL H_2O_2, catalyst, solvent: 1 mL EtOH and 3 mL water, rt. Entry (2), HMIL-100(Fe) – 2 mg catalyst. Entry (3), solid MIL-100(Fe) – 20 mg catalyst.

catalyst which was used for benzene to phenol oxidation (Table 1, entries 2 and 3).

Experimental section

According to Scheme 1, the freshly prepared sulfonated-PS spheres were dispersed alternately in an ethanolic solution of $FeCl_3{\cdot}6H_2O$ for 2 h and 1,3,5-benzenetricarboxylic acid (H_3BTC) for 2 h at 30 °C; between each step, the resulting products were collected by centrifugation and washed with ethanol. By repeating the growth cycle 5 times, we can achieve PS@aMIL-100(Fe) core–shell with the expected shell thickness. Then, the as synthesized nanoparticles (NPs) were adsorbed on the PS@aMIL-100(Fe) by stirring at room temperature for 1 h; subsequently PS@aMIL100(Fe)@Pt was centrifuged and washed twice with ethanol. In addition, further repeating of the growth cycle of the aMIL-100(Fe) coating with this core–shell can achieve a sandwich structure. A hollow sandwich structure was achieved by immersing the prepared PS@aMIL-100(Fe)@Pt@aMIL-100(Fe) into *N*,*N*-dimethylformamide (DMF) solvent to etch the polystyrene. The scanning electron microscopy (SEM) images (Fig. 1a) show that the uniform hollow MOFs have a diameter of approximately 416 nm. The shell thickness of about 30 nm was confirmed through transmission electron microscopy (TEM, Fig. 1c). The high angle annular dark-field scanning transmission electron microscopy (HAADF-STEM) images and the energy-dispersive X-ray spectroscopy (EDX) analysis show the well-dispersed C, H, O, Fe and Pt in the whole hollow amorphous structures (Fig. 1d). The same procedure was extended to synthesize different metal node hollow amorphous sandwich structures by replacing the Fe metal node with Cr, Al and Sc (Fig. S4–S6, ESI‡). In addition, Pt nanoparticles in PS@aMIL-100(Fe)@Pt@aMIL-100(Fe) were replaced with Rh and Ru nanoparticles to achieve different noble metal loaded hollow amorphous sandwich structures with an Fe metal node (Fig. 2). The powder X-ray diffraction (PXRD) patterns of the hollow MIL-100 series with different metal nodes shows their amorphous nature (Fig. S7, ESI‡)[46] The Brunauer–Emmett–Teller (BET) surface area was calculated to be 46 $m^2\ g^{-1}$ (Fig. S8, ESI‡).

The X-ray photoelectron spectroscopy (XPS) spectra of the Pt 4f regions for Pt nanoparticles and Pt/HMIL-100(Fe) are shown in Fig. 3a. Wherein the two characteristic peaks observed for the Pt NPs were at 71.5 and 74.8 eV, and for Pt loaded HMIL-100(Fe) the values were 71.8 and 75.1 eV. In addition, the binding energy shift of 0.3 eV to a higher position shows the electron donation from the Pt NPs to the supported HMIL-100(Fe). This result shows that the Pt was in an electron-deficient state which favored Fe^{3+} over $Fe^{2+/4+}$. Likewise, the Fe 2p spectra reveals that Fe^{3+} is found in HMIL-100(Fe). In addition, the binding energies of Fe 2p were found to be 714.5 & 727.9 eV in HMIL-100(Fe) and for HMIL-100(Fe)@Pt the values were 713.8 & 727.2 eV. Again, the lower binding energy shift of 0.7 eV in the Pt loaded HMIL-100(Fe)@Pt shows that electrons were transferred from the Pt NPs to the MOFs.

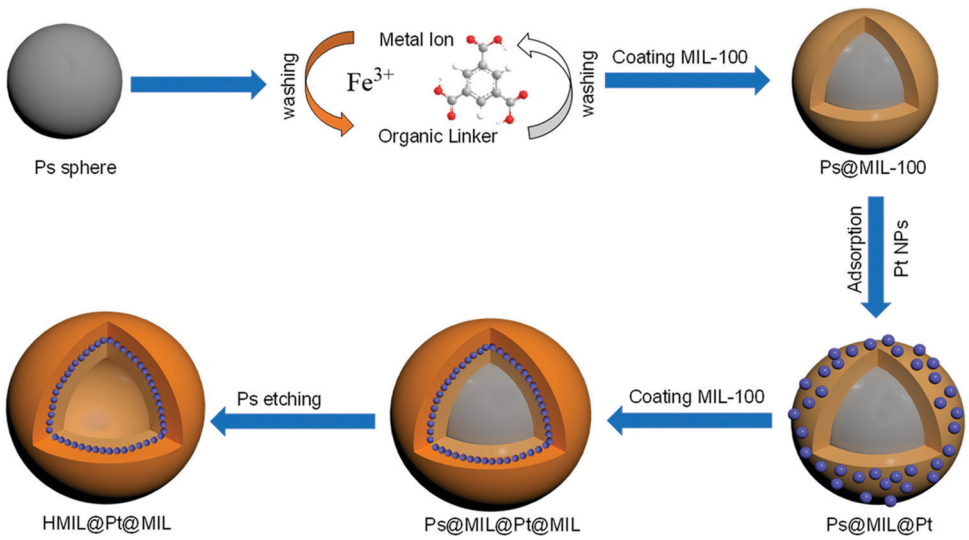

Scheme 1 Synthetic route to generate hollow sandwich aMIL-100@Pt@aMIL-100.

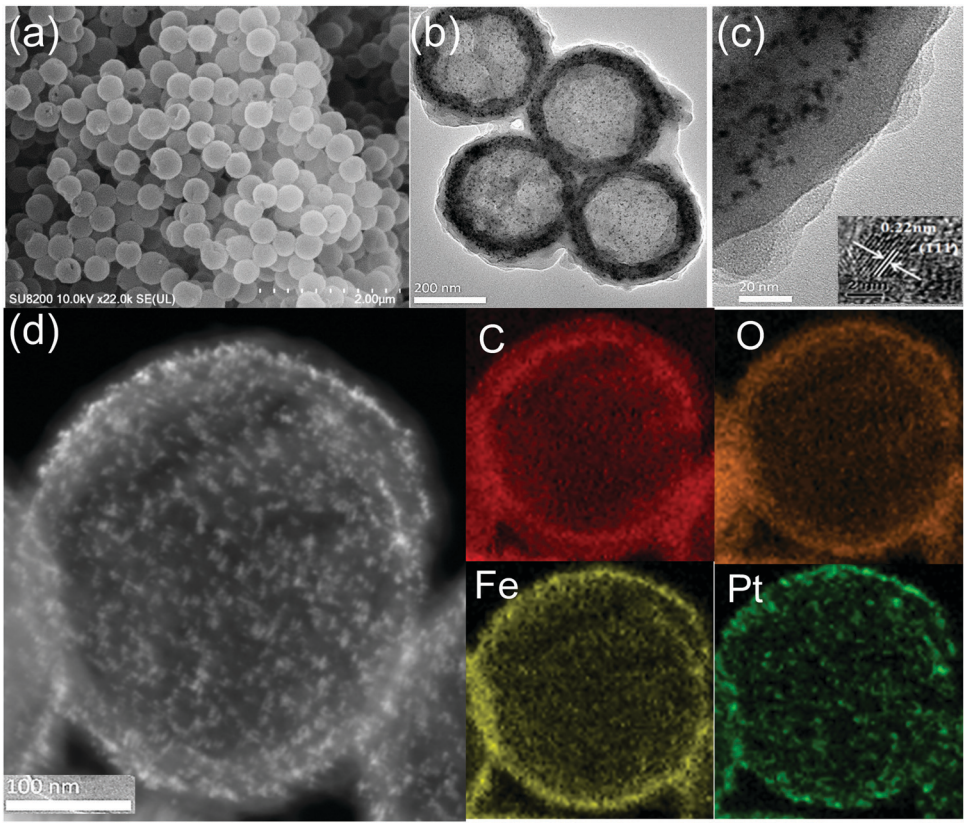

Fig. 1 HMIL-100(Fe)@Pt@aMIL-100(Fe) (a) SEM image, (b) large-scale TEM image and (c) magnified shell thickness. Inset: HRTEM image of Pt NPs. (d) HAADF-STEM image and EDS elemental mapping.

Results and discussion

The oxidation of benzene to phenol using H_2O_2 can be described by the equation

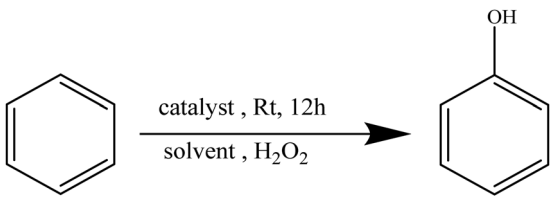

Table 1 summarizes the results obtained when using the hollow nanostructures as catalysts for the oxidation of benzene (A) to phenol (B).

The direct oxidation of benzene to phenol was carried out in the presence of catalyst X (where X is Pt, Rh or Ru) NPs with H_2O_2 as an oxidant at room temperature (Table 1, entry 1) and no conversion was observed. Then, we started exploring the reaction with HMIL-100(Fe) and solid MIL-100(Fe) (Table 1, entries 2 and 3) and low conversion with low selectivity was observed. So, to further enhance the activity of HMIL-100(X), where X stands for different metal nodes (Fe, Cr, Al and Sc), we have loaded Pt nanoparticles to form core shell HMIL-100(X)@Pt (where X is Fe, Cr, Al or Sc) (Table 1, entries 4–7) and among these catalysts HMIL-100(Fe)@Pt based on an Fe metal node shows moderate conversion with good selectivity due to the strong interaction and synergistic effect between Pt and the Fe metal node. We checked the TEM images after the reaction, which show that the core shell HMIL-100(X)@Pt catalysts (where X is Fe, Cr, Al or Sc) were unstable for this system (Fig. S9a, ESI‡). This inspired us to further coat other MOF shells to protect their stability (Table 1, entries 8–11) and we achieved good conversion with good selectivity for HMIL-100(Fe)@Pt@aMIL-100(Fe), which demonstrates that an Fe based metal node with Pt shows good conversion and selectivity; moreover, the sandwich structures show good stability. So, we directly achieved a different sandwich structured HMIL-100(Fe)@X@aMIL-100(Fe) with different noble metals (X is Rh or Ru). The Ru based HSMs (hollow sandwich aMOFs) showed lower conversion and selectivity than the Pt-based HSM. But, the Rh based HSM showed better conversion than the Pt-based HSM, with lower selectivity. This is due to the higher activity of Rh with H_2O_2, compared with all HSMs. Table 1, entry 11 shows that Pt nanoparticles enhance the activity of Fe based MOFs and control the selectivity in the benzene oxidation reaction. The HSM stability was checked from the TEM images after the reaction and they show that the HSM catalyst was stable for this system (Fig. S9b and c, ESI‡). Solvents played a vital role in this reaction; when water served as the reaction medium, the use of organic solvents was minimized, and among all the solvents investigated, the EtOH/H_2O mixed solvent 1 : 3 (mL/mL) resulted in the best performance by producing the

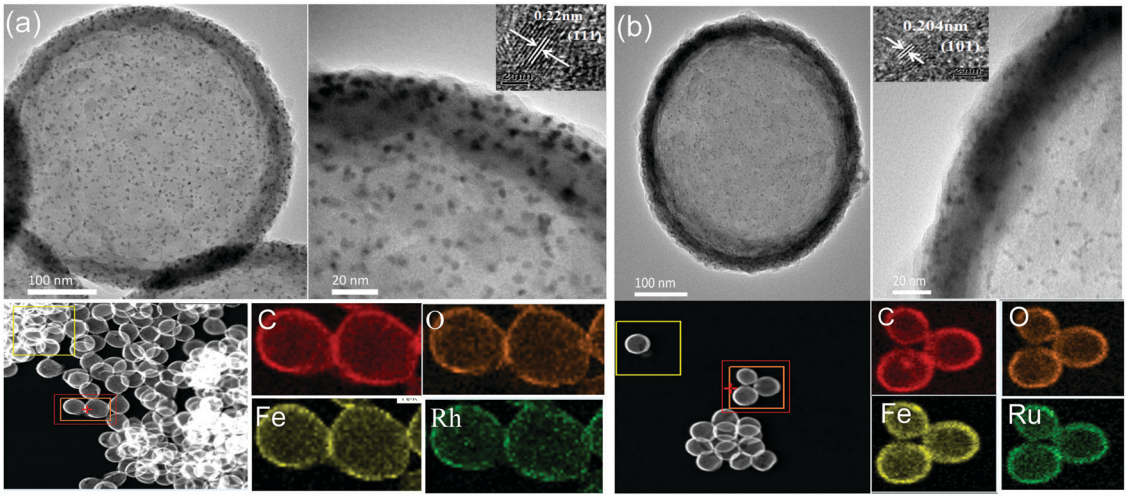

Fig. 2 TEM images and EDS elemental mapping of (a) HMIL-100(Fe)@Rh@aMIL-100(Fe) and (b) HMIL-100(Fe)@Ru@aMIL-100(Fe). Insets: HRTEM images of NPs (HAADF-STEM).

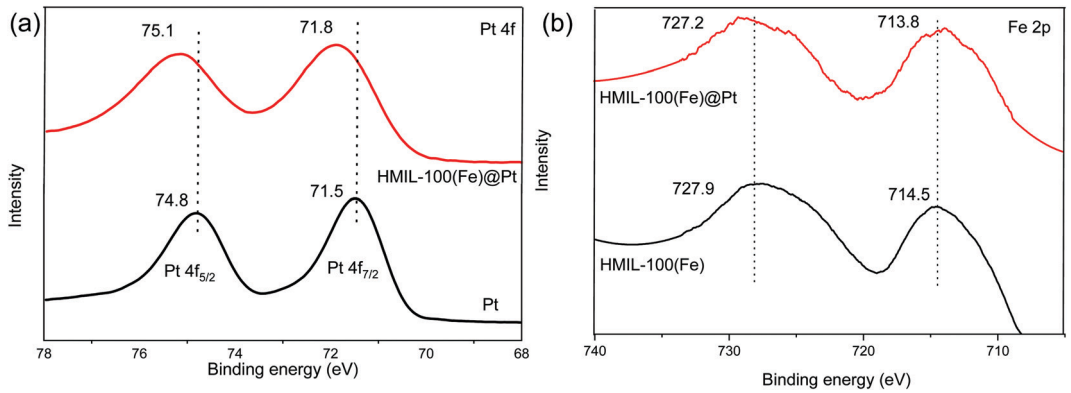

Fig. 3 XPS spectra of different samples in the (a) Pt 4f and (b) Fe 2p regions.

highest benzene conversion (Table S1, ESI‡). It is obvious that the reaction conducted in the mixed solvent was more effective for benzene conversion and phenol selectivity as compared with the single solvent systems, CH_3CN, EtOH or H_2O only. This is because in the biphasic system the benzene oxidation occurs in the aqueous phase in the cavity of the HMOFs because HMIL-100(Fe) is hydrophilic and it is easy for the aqueous phase component to diffuse into the cavities. Moreover, the presence of a suitable organic solvent not only increases the concentration of benzene in the aqueous phase, but is also favorable for the aqueous benzene oxidation reaction and extracts phenol production into the organic phase to minimize overoxidation of phenol by reducing the contact between phenol and the catalyst. For the catalytic stability, recycling experiments were performed. After each reaction, the catalyst was centrifuged, washed with ethanol and reused for the subsequent cycles. The catalyst showed no significant changes in terms of the catalytic activity and selectivity after successive reuses of up to three cycles (Fig. S10, ESI‡). The phase and morphology of the reused catalyst remained virtually unchanged relative to those of the fresh catalyst (Fig. S9b and c, ESI‡), which also verified the stability of the catalyst.

We explored whether H_2O_2 could be activated on the Fe site and if the noble metal (Pt, Rh or Ru) NPs could accelerate the process of converting H_2O_2 to OH. However, directly elucidating this synergetic effect is very difficult. Deng *et al.* reported that an additional H_2O_2 can also create a second adsorbed oxygen species on an Fe single atom catalyst with one oxygen preabsorbed and oxidize benzene.[44] Also, Zhang *et al.* reported that an SA-Fe/CN catalyst can dissociate H_2O_2 into two hydroxyls ($2HO^{\bullet}$), coadsorbing at the single Fe site in accordance with recent theoretical density functional theory (DFT) calculations.[47] The observed formation of Fe^{IV}=O species, usually considered to be the active intermediates in this kind of reaction, verifies that H_2O_2 could be activated on the Fe atom. These two works support our understanding of the reactivity of this reaction. For further confirmation, we carried out spin trapping in EPR studies using 5,5-dimethyl-1-pyrroline *N*-oxide (DMPO); this is one of the most popular spin traps and the EPR features of its spin adducts are well established. For example, the EPR spectrum of the HO radical adduct (DMPO OH) exhibits signals with a relative peak ratio of 1 : 2 : 2 : 1. The hyperfine splitting pattern of the observed radical clearly indicates that HO is

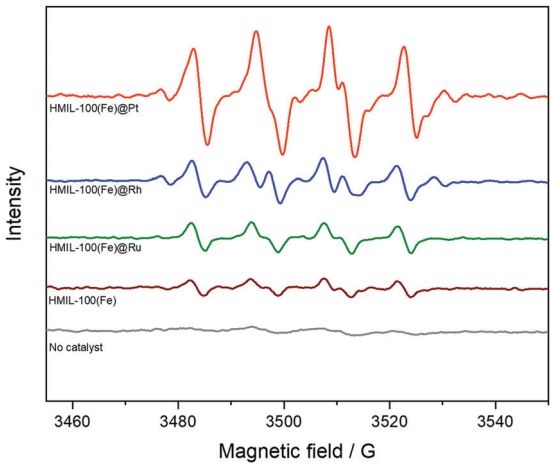

Fig. 4 EPR spectra recorded during the oxidation of benzene with H_2O_2 in the presence of various catalysts and DMPO.

produced during the reaction of benzene with H_2O_2 and HMIL and is trapped by DMPO to produce DMPO–OOH. It was further confirmed that the addition of DMPO to a methanol solution of benzene and H_2O_2 without a catalyst (HMIL) resulted in no observation of an EPR signal. The results indicated that the intensities of the EPR spectra were of the order of HMIL@Pt > HMIL@Rh > HMIL@Ru > HMIL > no catalyst (Fig. 4). In summary, when the catalyst was added to the methanol solution of benzene, H_2O_2 and DMPO, a strong EPR signal assigned to DMPO–OOH was observed, which suggested that more OH radicals were produced by the Pt-based catalyst.

Here, we propose a plausible mechanism for the benzene oxidation reaction based on our experimental results. The aromaticity and delocalized pi system in benzene and slow production of hydroxyl radicals result in an uncatalyzed benzene oxidation reaction, which is kinetically slow. Therefore, decreasing the stability of benzene and facilitating the yield of hydroxyl radicals are efficient approaches to increase the reaction rate to achieve high yield.

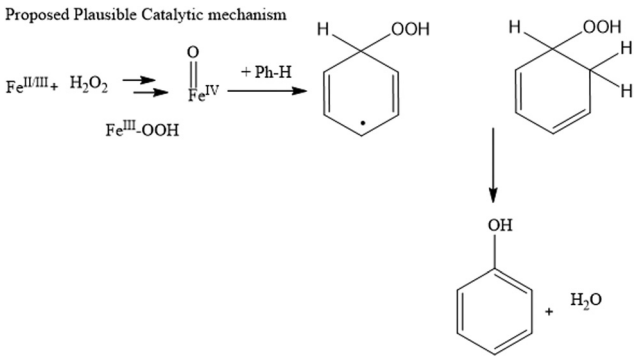

Conclusion

In conclusion, we have synthesized amorphous hollow sandwich MIL-100 MOFs through a step-by-step assembly strategy. The catalytic oxidation of benzene indicates that the well-designed amorphous hollow sandwich structure contributes to the excellent catalytic performance and selective production of phenol and also reduced catalyst loading, relative to that of the solid MOFs. This work may reveal new opportunities for the industrial production of commodity chemicals.

Conflicts of interest

There are no conflicts to declare.

Acknowledgements

The author gratefully acknowledges the financial support from the CAS-TWAS President's fellowship of the National Center for Nanoscience and Technology (NCNST) under the University of Chinese Academy of Sciences (UCAS) and Professor Zhiyong Tang.

References

1 O. M. Yaghi, M. J. Kalmutzki and C. S. Diercks, *Introduction to Reticular Chemistry: Metal-Organic Frameworks and Covalent Organic Frameworks*, John Wiley & Sons, 2019.
2 O. M. Yaghi, *ACS Cent. Sci.*, 2019, **5**, 1295–1300.
3 O. M. Yaghi, *J. Am. Chem. Soc.*, 2016, **138**, 15507–15509.
4 V. Srinivasapriyan, *Anal. Methods*, 2020, **12**, 4635–4637.
5 C. H. Hendon, A. J. Rieth, M. D. Korzyński and M. Dincă, *ACS Cent. Sci.*, 2017, 3, 554–563.
6 J. Lee, O. K. Farha, J. Roberts, K. A. Scheidt, S. T. Nguyen and J. T. Hupp, *Chem. Soc. Rev.*, 2009, **38**, 1450–1459.
7 J. Gascon, A. Corma, F. Kapteijn and F. X. Llabrés i Xamena, *ACS Catal.*, 2014, **4**, 361–378.
8 D. Yang and B. C. Gates, *ACS Catal.*, 2019, **9**, 1779–1798.
9 V. Srinivasapriyan, *Nanoscale Adv.*, 2019, **1**, 3379–3382.
10 V. Srinivasapriyan, *Mater. Adv.*, 2020, **1**, 326–328.
11 H. Kim, S. Yang, S. R. Rao, S. Narayanan, E. A. Kapustin, H. Furukawa, A. S. Umans, O. M. Yaghi and E. N. Wang, *Science*, 2017, **356**, 430–434.
12 M. J. Kalmutzki, C. S. Diercks and O. M. Yaghi, *Adv. Mater.*, 2018, **30**, 1704304.
13 Y. Tu, R. Wang, Y. Zhang and J. Wang, *Joule*, 2018, **2**, 1452–1475.
14 S. M. T. Abtab, D. Alezi, P. M. Bhatt, A. Shkurenko, Y. Belmabkhout, H. Aggarwal, Ł. J. Weseliński, N. Alsadun, U. Samin and M. N. Hedhili, *Chem*, 2018, **4**, 94–105.
15 K. J. Hartlieb, J. M. Holcroft, P. Z. Moghadam, N. A. Vermeulen, M. M. Algaradah, M. S. Nassar, Y. Y. Botros, R. Q. Snurr and J. F. Stoddart, *J. Am. Chem. Soc.*, 2016, **138**, 2292–2301.
16 J. Liu, D. Zhu, C. Guo, A. Vasileff and S. Z. Qiao, *Adv. Energy Mater.*, 2017, **7**, 1700518.
17 G. Liu, V. Chernikova, Y. Liu, K. Zhang, Y. Belmabkhout, O. Shekhah, C. Zhang, S. Yi, M. Eddaoudi and W. J. Koros, *Nat. Mater.*, 2018, **17**, 283–289.
18 P. Falcaro, R. Ricco, C. M. Doherty, K. Liang, A. J. Hill and M. J. Styles, *Chem. Soc. Rev.*, 2014, **43**, 5513–5560.

19 J. Zhao, H. Li, C. Li, Q. Zhang, J. Sun, X. Wang, J. Guo, L. Xie, J. Xie and B. He, *Nano Energy*, 2018, **45**, 420–431.
20 Z. Zhang, Y. Chen, X. Xu, J. Zhang, G. Xiang, W. He and X. Wang, *Angew. Chem., Int. Ed.*, 2014, **53**, 429–433.
21 D. Cai, B. Liu, D. Wang, L. Wang, Y. Liu, B. Qu, X. Duan, Q. Li and T. Wang, *J. Mater. Chem. A*, 2016, **4**, 183–192.
22 Z. X. Cai, Z. L. Wang, J. Kim and Y. Yamauchi, *Adv. Mater.*, 2019, **31**, 1804903.
23 Z. Zhang, Y. Chen, S. He, J. Zhang, X. Xu, Y. Yang, F. Nosheen, F. Saleem, W. He and X. Wang, *Angew. Chem., Int. Ed.*, 2014, **53**, 12517–12521.
24 Z. Wang, N. Yang and D. Wang, *Chem. Sci.*, 2020, **11**, 5359–5368.
25 W. Zhu, Z. Chen, Y. Pan, R. Dai, Y. Wu, Z. Zhuang, D. Wang, Q. Peng, C. Chen and Y. Li, *Adv. Mater.*, 2019, **31**, 1800426.
26 T. D. Bennett, A. L. Goodwin, M. T. Dove, D. A. Keen, M. G. Tucker, E. R. Barney, A. K. Soper, E. G. Bithell, J.-C. Tan and A. K. Cheetham, *Phys. Rev. Lett.*, 2010, **104**, 115503.
27 T. D. Bennett and A. K. Cheetham, *Acc. Chem. Res.*, 2014, **47**, 1555–1562.
28 J. Fonseca and S. Choi, *Microporous Mesoporous Mater.*, 2021, **310**, 110600.
29 A. F. Sapnik, I. Bechis, S. M. Collins, D. N. Johnstone, G. Divitini, A. J. Smith, P. A. Chater, M. A. Addicoat, T. Johnson and D. A. Keen, *Nat. Commun.*, 2021, **12**, 2062.
30 W. Liu, J. Huang, Q. Yang, S. Wang, X. Sun, W. Zhang, J. Liu and F. Huo, *Angew. Chem., Int. Ed.*, 2017, **56**, 5512–5516.
31 Y. Qin, X. Han, Y. Li, A. Han, W. Liu, H. Xu and J. Liu, *ACS Catal.*, 2020, **10**, 5973–5978.
32 M. Weber, M. Weber and V. Weber, *Ullmann's Encyclopedia of Industrial Chemistry*, 2021, DOI: 10.1002/14356007.a19_299.pub3.
33 R. J. Schmidt, *Appl. Catal., A*, 2005, **280**, 89–103.
34 S.-I. Niwa, M. Eswaramoorthy, J. Nair, A. Raj, N. Itoh, H. Shoji, T. Namba and F. Mizukami, *Science*, 2002, **295**, 105–107.
35 Z. Chen, J. Mao and R. Zhou, *Appl. Surf. Sci.*, 2019, **465**, 15–22.
36 Y. Liu, K. Murata and M. Inaba, *J. Mol. Catal. A: Chem.*, 2006, **256**, 247–255.
37 R. Bal, M. Tada, T. Sasaki and Y. Iwasawa, *Angew. Chem., Int. Ed.*, 2006, **45**, 448–452.
38 G. Panov, *CATTECH*, 2000, **4**, 18–31.
39 L. Pirutko, V. Chernyavsky, A. Uriarte and G. Panov, *Appl. Catal., A*, 2002, **227**, 143–157.
40 J. Jia, K. S. Pillai and W. M. Sachtler, *J. Catal.*, 2004, **221**, 119–126.
41 L. Balducci, D. Bianchi, R. Bortolo, R. D'Aloisio, M. Ricci, R. Tassinari and R. Ungarelli, *Angew. Chem., Int. Ed.*, 2003, **42**, 4937–4940.
42 J. Zhang, Y. Tang, G. Li and C. Hu, *Appl. Catal., A*, 2005, **278**, 251–261.
43 G. Wen, S. Wu, B. Li, C. Dai and D. S. Su, *Angew. Chem., Int. Ed.*, 2015, **54**, 4105–4109.
44 D. Deng, X. Chen, L. Yu, X. Wu, Q. Liu, Y. Liu, H. Yang, H. Tian, Y. Hu and P. Du, *Sci. Adv.*, 2015, **1**, e1500462.
45 Y. Morimoto, S. Bunno, N. Fujieda, H. Sugimoto and S. Itoh, *J. Am. Chem. Soc.*, 2015, **137**, 5867–5870.
46 A.-L. Li, F. Ke, L.-G. Qiu, X. Jiang, Y.-M. Wang and X.-Y. Tian, *CrystEngComm*, 2013, **15**, 3554–3559.
47 M. Zhang, Y.-G. Wang, W. Chen, J. Dong, L. Zheng, J. Luo, J. Wan, S. Tian, W.-C. Cheong and D. Wang, *J. Am. Chem. Soc.*, 2017, **139**, 10976–10979.